CHAPTER SIX

Probing the Electrochemical Behaviour of SWCNT-Cobalt Nanoparticles and Their Electrocatalytic Activities Towards the Detection of Nitrite in Acidic and Physiological pH Conditions*

* The following publications resulted from part of the research work presented in this chapter and are not referenced further in this thesis:

5. **Abolanle S. Adekunle**, Jeseelan Pillay, Kenneth I. Ozoemena, *Electrochim. Acta* 55 (2010) 4319-4327.
6. **Abolanle S. Adekunle**, Kenneth I. Ozoemena, *Int. J. Electrochem. Sci.* (in press).

6.1. Comparative FESEM, AFM images EDX spectra

Figure 6.1 showed the comparative scanning electron microscopy (SEM) images of the EPPGE, EPPGE-SWCNT, EPPGE-SWCNT-Co and EPPGE-SWCNT-CoO. Upon electro-deposition of Co nanoparticles, EPPGE-SWCNT-Co modified electrode was formed (Fig 6.1c). There is high dispersion of Co nanoparticles, possibly made due to the strong electrostatic interactions between the Co^{2+} ions in solution and the COO^- charge of the SWCNTs on the electrode surface. The Co nanoparticles form a porous and high electroactive material on the electrode surface but with several interstitial spaces or voids. Repetitive cycling (20 scans) of EPPGE-SWCNT-Co electrode in 0.1 M phosphate buffer solution, PBS (pH 7.0) gave EPPGE-SWCNT-CoO modified electrode in which the cobalt particles formed a thick amorphous film (Fig. 6.1d) with little voids. AFM topographic heights (not shown) increased from 14 nm for bare substrate to 80 nm on integrating with SWCNTs and finally to 120 nm on incorporation with cobalt or its oxides. Salimi *et al.* [1,2] employed similar method of electrode decoration with cobalt oxide nanoparticles and observed particles agglomeration with sizes ranging from 100 – 600 nm. As evident from the cross-sections (Figures 6.1g and h), the particle sizes are in the 8 – 30 nm range, suggesting some agglomeration of the nanoparticles.

Figure 6.2 is the EDX profile of the electrodes. The EPPGE electrode (a) was purely carbon (~ 100%) as would be expected for pure graphite surface. The presence of oxygen peaks in the EPPGE-SWCNT (b) is an indication of the successful modification of the SWCNT to the acid derivatives SWCNT-COOH while the sulphur peak can be attributed to the sulphuric acid used during treatment.

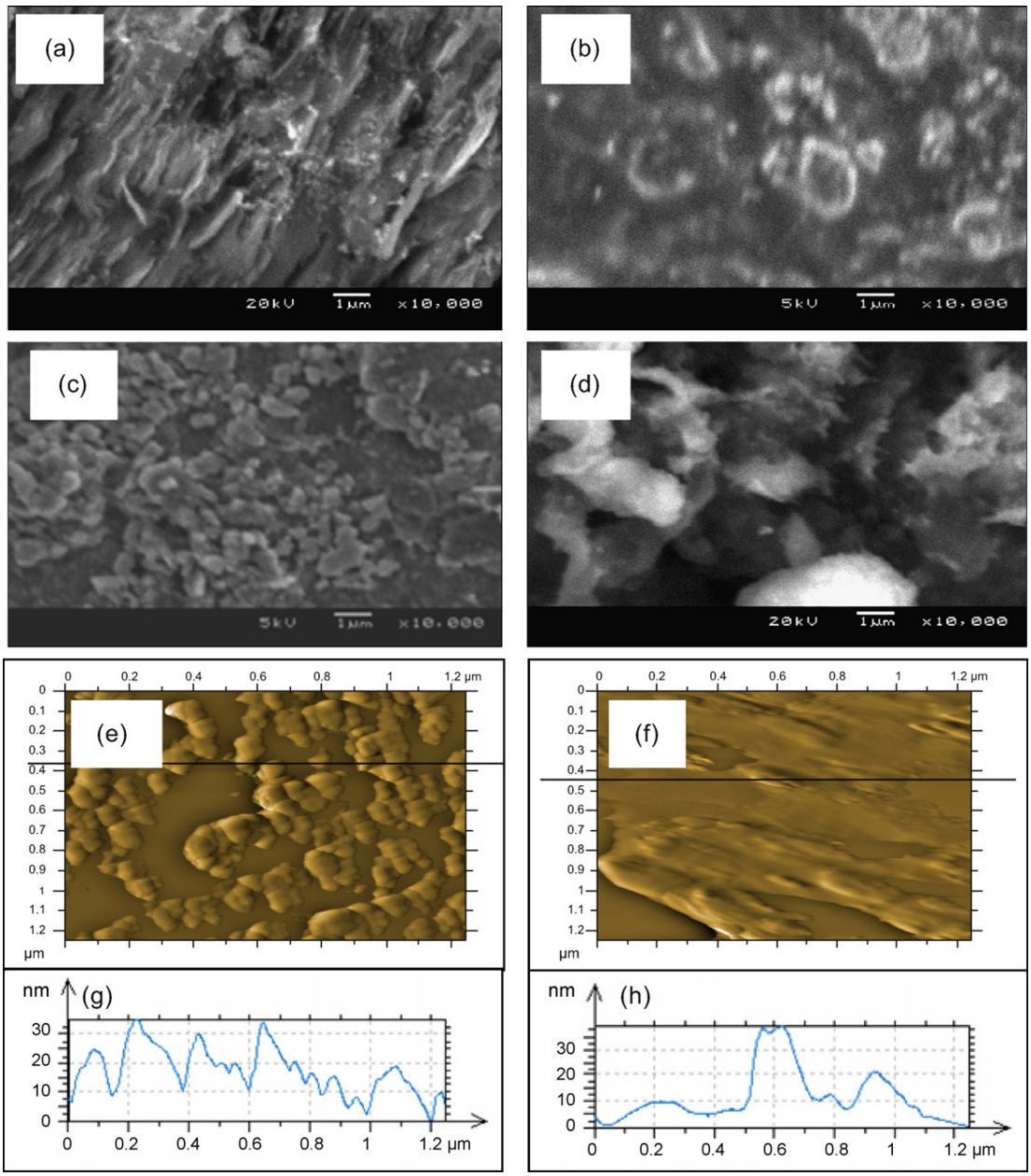

Figure 6.1: FESEM of (a) EPPGE, (b) EPPGE-SWCNT, (c) EPPGE-SWCNT-Co, (d) EPPGE-SWCNT-CoO. (e) and (f) are the AFM topography images for the EPPGE-SWCNT-Co and the EPPGE-SWCNT-CoO while (g) and (h) are their respective cross-sections.

EPPG-SWCNT-CoO (c) showed the presence of Co and oxygen peaks with very pronounced intensity implying that the electrode was successfuly modified with CoO nanoparticles. The occurrence of P and Na peaks in the EDX of EPPGE-SWCNT-CoO may be attributed to the sodium phosphate buffer solution used for the electrode treatment.

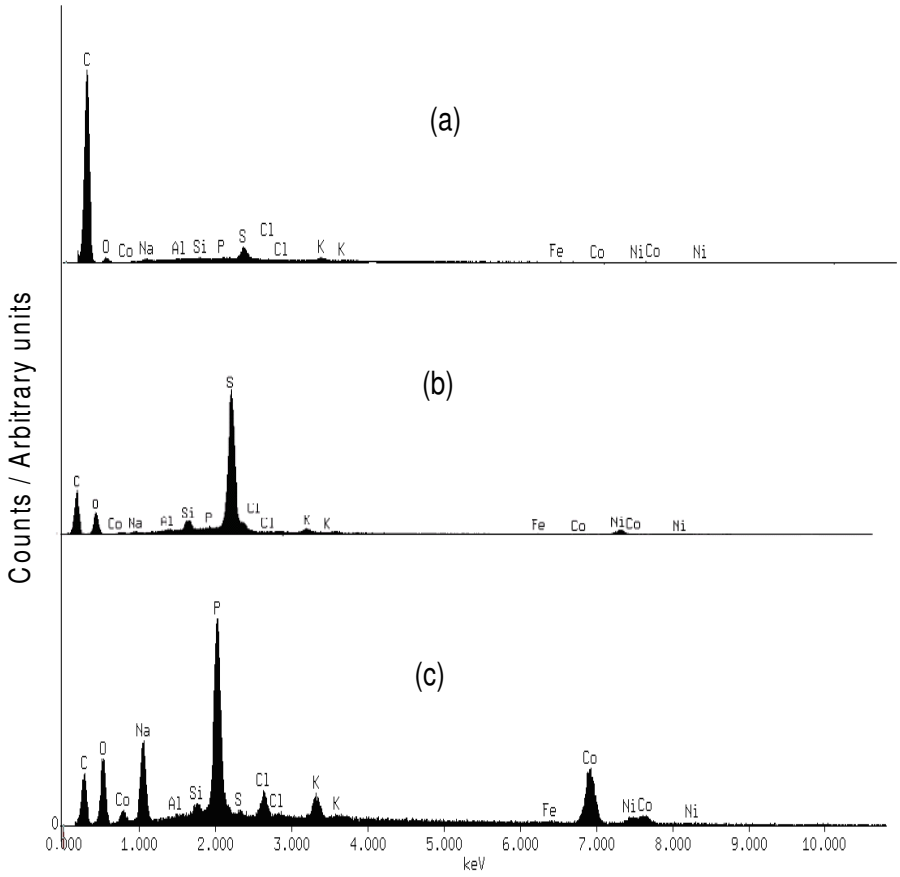

Figure 6.2: EDX spectra of (a) EPPGE (b) EPPGE-SWCNT, and (c) EPPGE-SWCNT-CoO.

6.2 Comparative Electrochemical characterization

Comparative current response (not shown) of bare-EPPGE, EPPGE-Co, EPPGE-CoO, EPPGE-SWCNT, EPPGE-SWCNT-Co and EPPG-SWCNT-CoO in PBS (pH 7.0) was investigated. From the cyclic voltammograms (not shown), the anodic peak at 0.68 V and its corresponding cathodic peak at around 0.46 V are attributed to Co(II)/Co(III) which has been reported to be at 0.7 to 0.8 V (vs SCE) [3-5] in an acidic medium. The anodic peak at 0.68 V vs Ag|AgCl, sat'd KCl (~ 0.64 V vs SCE) is close to 0.6 V vs SCE reported by Salimi et al. [2] and was attributed to the formation of Co_3O_4 through the reaction below:

$$3Co(OH)_2 + 2OH^- \longrightarrow Co_3O_4 + 4H_2O + 2e^- \quad (6.1)$$

Another anodic peak was observed at around +1.0 V, also observed by others [2] at 0.95 V and assigned to COOH formation as a result of oxidation of $Co(OH)_2$ or the Co_3O_4 as represented by the equations below:

$$Co(OH)_2 + OH^- \longrightarrow CoOOH + H_2O + e^- \quad (6.2)$$

$$Co_3O_4 + H_2O + OH^- \longrightarrow 3CoOOH + e^- \quad (6.3)$$

Sunohara *et al.* [6] reported the peak at potential >1.0 V (vs Ag|AgCl) and attributed it to the Co_2O_3 / Co_3O_4 redox process. A cathodic peak was also observed at ca 0.72V and is attributed to the reduction of CoOOH to $Co(OH)_2$ or Co_3O_4. Peak at around - 0.2 V (vs Ag|AgCl, sat'd KCl) is due to Co^{2+}/Co redox process, similar to that observed by others [2] at around - 0.1 V (vs SCE) on a cobalt oxide nanoparticles modified glassy carbon electrode. The current

responses of these electrodes increase in this order: EPPGE-SWCNT-Co > EPPGE-SWCNT-CoO > EPPGE-Co > EPPGE-CoO > EPPGE-SWCNT > bare-EPPGE.

The result indicates that: (i) deposition of SWCNT on the bare–EPPGE enhances its electron transfer since SWCNTs could be acting as the conducting electrical nanowires for the flow of electrons; (ii) enhanced current response was observed when the cobalt nanoparticles were integrated with the SWCNTs, implying a positive synergistic behaviour between these two nanomaterials; and (iii) the SWCNT-Co modified electrodes gave higher current responses with decreased peak-to-peak separation potential (ΔEp = 0.23 V) compared with those without SWCNT (ΔE = 0.32 V). It is therefore reasonable to suggest that SWCNTs enhance the electrochemical response of the modified electrodes by serving as the conducting nanowires for electron transfer between the Co nanoparticles and the underlying EPPGE.

6.3 Comparative electron transport properties

The aim of this experiment was to explore the extent to which the modifiers allow the electron transport between $Fe(CN)_6]^{4-}$ / $[Fe(CN)_6]^{3-}$ redox probe and the base EPPGE. The CV experiments were performed in 5 mM $Fe(CN)_6]^{4-}$ / $[Fe(CN)_6]^{3-}$ solution (in PBS pH 7.0). The peaks in the 0 – 0.4 V region is due to the $Fe(CN)_6]^{4-}$ / $[Fe(CN)_6]^{3-}$ redox couple while the one at the 0.4 – 1.0 V region is ascribed to the Co(II)/Co(III) redox process (Figure 6.3).

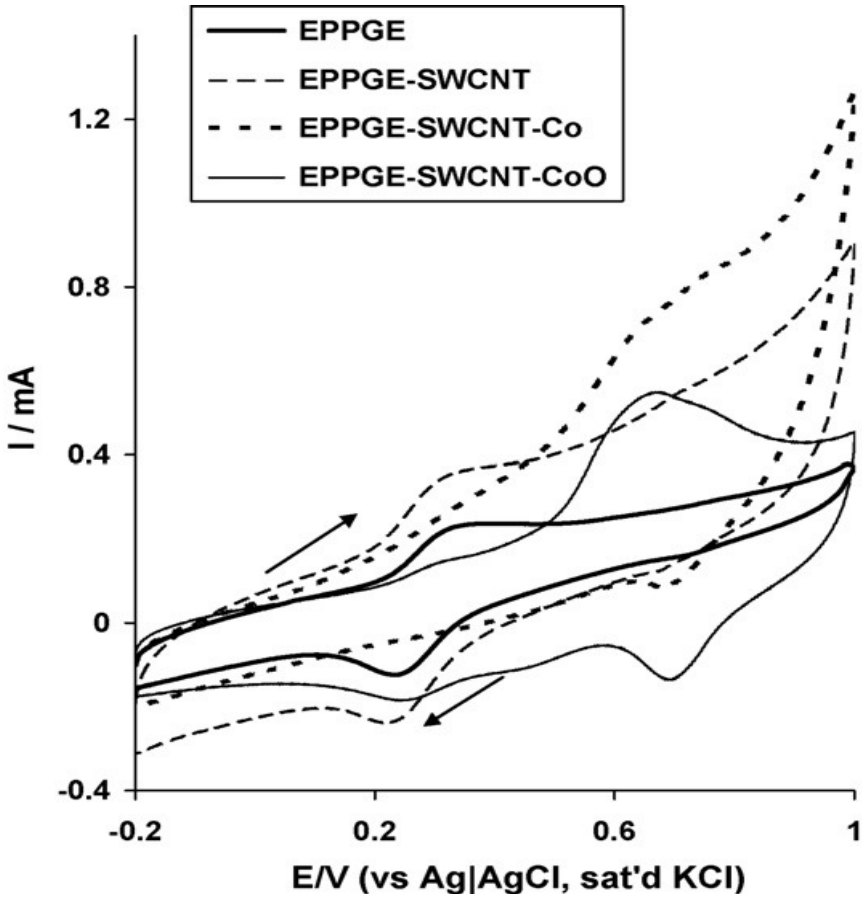

Figure 6.3: Typical examples of some cyclic voltammetric evolutions of the electrodes in 5 mM $[Fe(CN)_6]^{4-}$ / $[Fe(CN)_6]^{3-}$ solution (PBS pH 7.0). Scan rate = 50 mV/s.

For further understanding of the electronic behaviour of the SWCNT and SWCNT-Co modified electrodes (EPPGE-SWCNT, EPPGE-SWCNT-Co, EPPGE-SWCNT-CoO), EIS study in $Fe(CN)_6]^{4-}$ / $[Fe(CN)_6]^{3-}$ solution was carried out at the equilibrium potential of the redox couple ($E_{1/2}$ of 0.3 V) as seen in Figure 6.4. The impedance technique is a very sensitive technique which gives insight into the mechanism of the electron transport between the

electrode|electrolyte interface. The Nyquist plots for some of the electrodes are presented in Figure 6.4a.

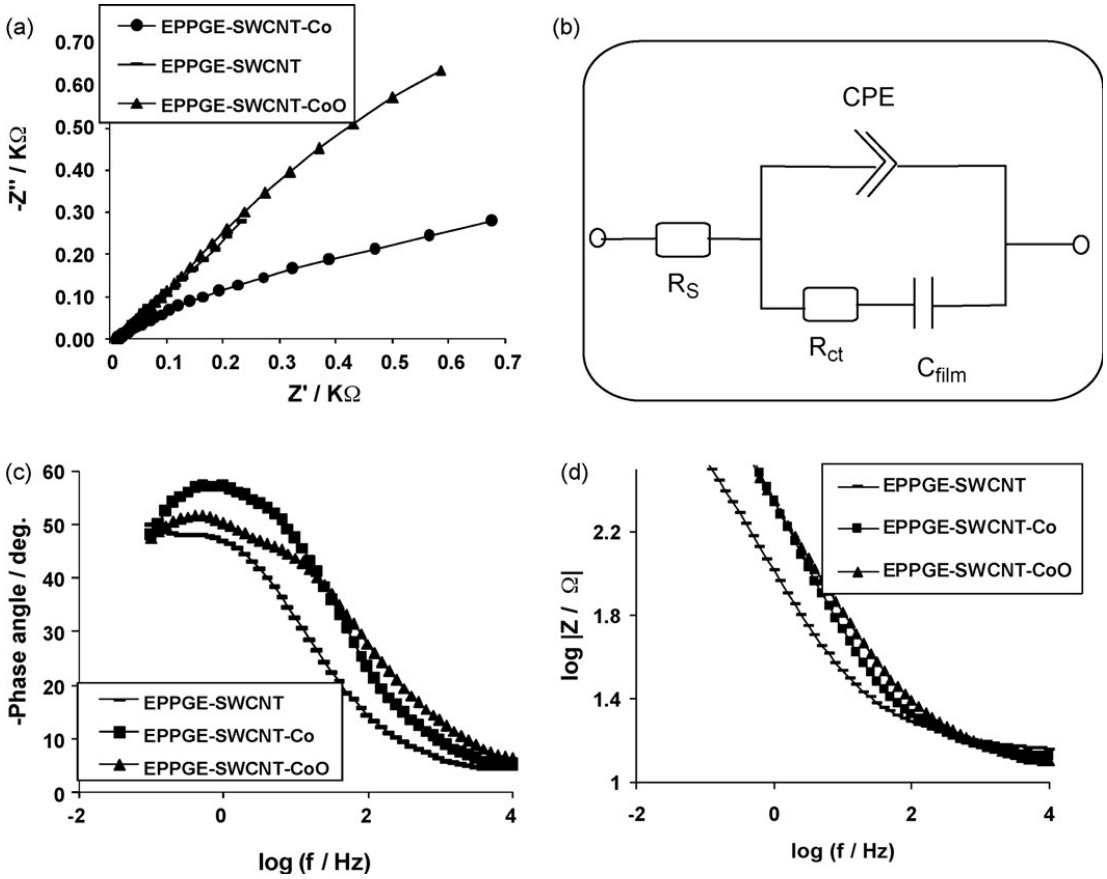

Figure 6.4: (a) Typical Nyquist plots of some of the electrodes obtained in 5 mM $[Fe(CN)_6]^{4-}$ / $[Fe(CN)_6]^{3-}$ solution (PBS pH 7.0) at fixed potential of 0.30 V vs Ag|AgCl sat'd KCl. (b) Represents the circuit used in the fitting of the EIS data. (c) and (d) are the Bode plots obtained for the electrodes, showing the plots of (-phase angle deg. vs log (f/Hz)) and log |Z / Ω| vs log (f/Hz).

The EIS data was satisfactorily fitted with the modified Dolin-Ershler equivalent circuit model (Figure 6.4b) [7], judged by the values of the pseudo χ^2 and relative % errors (Table 6.1) as well as

the goodness of fit (Figure 6.4a) wherein the true capacitance (C_{dl}) is replaced by the constant phase element (CPE). R_s, R_{ct} and C_{film} are already defined. The passive layer formed by the EPPGE-SWCNT-CoO leads to an insulated surface which could be responsible for the high R_{ct} value. It is evident from this study that the EPPGE-SWCNT-Co has the least R_{ct} value indicating faster electron transport. Circuit 6.4b description is different from the circuit used in earlier report involving SWCNT/Ni probably because of the porous nature of the EPPGE which alters its electronic properties with use [8]. The relatively low R_{ct} for the SWCNT-Co indicates faster electron transport compared to the other electrodes, possibly as a result of the porous and the high electroactive surface area of the electrode which allows for easy contact between the electrolyte and the base EPPGE. The high R_{ct} value for the SWCNT-Co_3O_4 is attributed to the formation of a thick cobalt oxide nanoparticles films which increase in thickness as the number of scans increases during modification. As has elegantly been described by the recent work of Orazem and Tribollet [9], time-constant (or frequency) dispersions leading to CPE behaviour occur as a result of distribution of time constants along either the area of the electrode surface (involving a 2-dimensional aspect of the electrode) or along the axis normal to the electrode surface (involving a 3-dimensional surface). Importantly, a 2-D distribution presents itself as an ideal RC behaviour, meaning that impedance measurements are very useful in distinguishing whether the observed global CPE behaviour is due to a 2-D distribution, from a 3-D distribution, or from a combined 2-D and 3-D distributions. It may be concluded that the observed impedimetric behaviour of the electrodes is a combination of 2-D and 3-D distributions.

Table 6.1: Impedance data obtained for the EPPGE modified electrodes in 5 mM $[Fe(CN)_6]^{4-}$ / $[Fe(CN)_6]^{3-}$ solution (PBS pH 7.0) at 0.30 V vs Ag|AgCl sat'd KCl.

Electrodes	**Impedimetric Parameters**					
	R_s / Ω cm^2	**CPE / mF**	**n**	**R_{ct} / Ω cm^2**	**C / µF**	**χ^2**
EPPGE-SWCNT	3.23 ±0.01	3.56 ±0.03	~ 0.56	12.93±0.33	135.00±12.12	2.55x10^{-3}
EPPGE-SWCNT-Co	2.93 ±0.02	1.32±0.02	~ 0.62	8.72±0.22	75.80±9.38	7.50 x10^{-5}
EPPGE-SWCNT-CoO	1.24±0.01	1.56±0.01	~ 0.57	17.96±0.25	22.07±4.12	9.50 x10^{-4}

From the plot of log |Z| vs log f, Figure 6.4d, the higher slope value (-0.65, R^2 = 0.9997 for EPPGE-SWCNT-Co) compared with -0.57, R^2 = 0.9991 for EPPGE-SWCNT-Co_3O_4 and -0.52, R^2 = 0.9988 for EPPGE-SWCNT suggests the more capacitive nature of EPPGE-SWCNT-Co than its oxide and the SWCNT counterparts. From the other type of Bode plot (i.e., –phase angle vs log f, (Figure 6.4c), the phase angles were 65^0 for EPPGE-SWCNT-Co compared with the EPPGE-SWCNT-CoO (51^0) and EPPGE-SWCNT (48^0), which are less than the 90^o expected of an ideal capacitive behaviour confirming the presence of CPE and pseudocapacitive nature of these electrodes.

6.4 Electrocatalytic oxidation of Nitrite in neutral and acidic pH

Figure 6.5 presents the current responses of the modified electrodes in 10^{-3} M NO_2^- in PBS pH 7.4 and pH 3.0, respectively. The nitrite exists as nitrite ion (NO_2^-) in pH 7.4 PBS and at slightly acidic pH, the nitrite ion disproportionate to produce the neutral nitric oxide (NO) [10], which has a very short life time especially in an air saturated condition. Thus, the solution under the acidic pH was prepared fresh, with nitrogen purged, de-aerated phosphate buffer solution before analysis. The current response of the EPPGE-SWCNT-Co towards nitrite at pH 7.4 was approximately 3 folds higher than the other electrodes (Figure 6.5a) with slightly lower onset potentials (0.78 V). At pH 3.0 the EPPGE-SWCNT-Co exhibits faster calaysis compared to EPPGE-Co (less positive potential, ~ 100 mV lower than Co electrodes without SWCNTs), but the current response was almost the same.

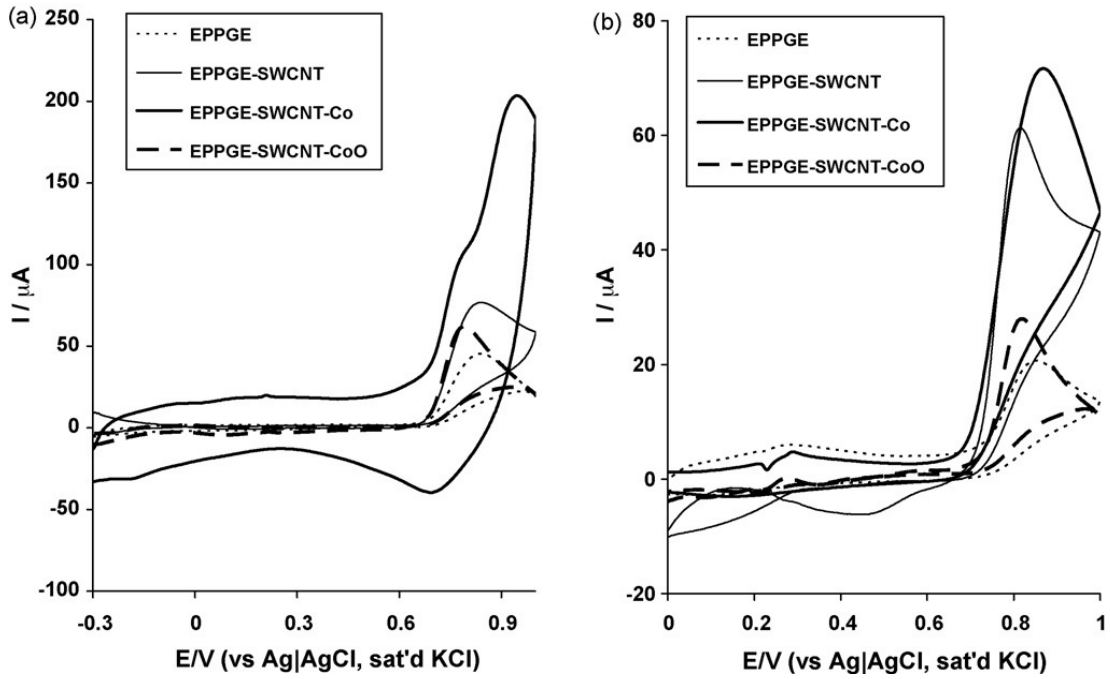

Figure 6.5: Comparative current response (after background current subtraction) of the EPPGE, EPPGE- SWCNT, EPPGE-SWCNT-Co and EPPGE-SWCNT-CoO in (a) 1 mM nitrite solution in pH 7.4 PBS and (b) 1 mM nitrite solution in pH 3.0 PBS, scan rate = 25 mV/s.

Cobalt modified electrodes have been reported to give enhanced response towards electro-oxidation of nitrite on graphite substrate [6,11,12] and on gold modified electrode [13,14]. It is evident from Figure 6.5a that the oxidation potential was lower with high current response on the EPPGE-SWCNT-Co nanoparticles modified electrode prepared by electrodeposition. The better electro-oxidation reaction of the SWCNT modified electrodes especially the EPPGE-SWCNT-Co, can be attributed to the SWCNT itself acting as an electrical conducting nanowire which enhances electron transport between the base electrode and the analyte. Since EPPGE-SWCNT-Co proved to be the best electrode towards nitrite oxidation at the pH conditions

investigated, all further studies were carried out with it, unless otherwise stated.

6.5 Electrochemical impedance studies

Figure 6.6a presents the Nyquist plots for the electrochemical impedance (EIS) data obtained at the electrodes studied during the electrocatalytic oxidation of nitrite (in pH 7.4 PBS) at a fixed potential of 0.8 V vs Ag|AgCl, sat'd KCl. The results obtained for the oxidation of the analyte at pH 3.0 PBS follow similar trend (not shown). A circuit model (Figure 6.6b) which incorporates the constant phase element (CPE) and an inductor *L,* yielded satisfactory results with acceptable values of pseudo χ^2 and % error values (Table 6.2). This suggests that there may be adsorption of the oxidation product on the electrodes. Thus, the CPE with *n* values of 0.73 and 0.87 suggest pseudocapacitive properties occuring at the electrode|solution interface. In electrocatalytic reactions, it is known that inductive behaviour takes place when the Faradaic current is governed by the occupation of an intermediate state [15-17]. This adsorption phenomenon is expected since CNT used as part of the electrode modifier, is known for adsorption properties because of their high surface area. This is the first time the adsorption associated with nitrite oxidation is proven by EIS measurement.

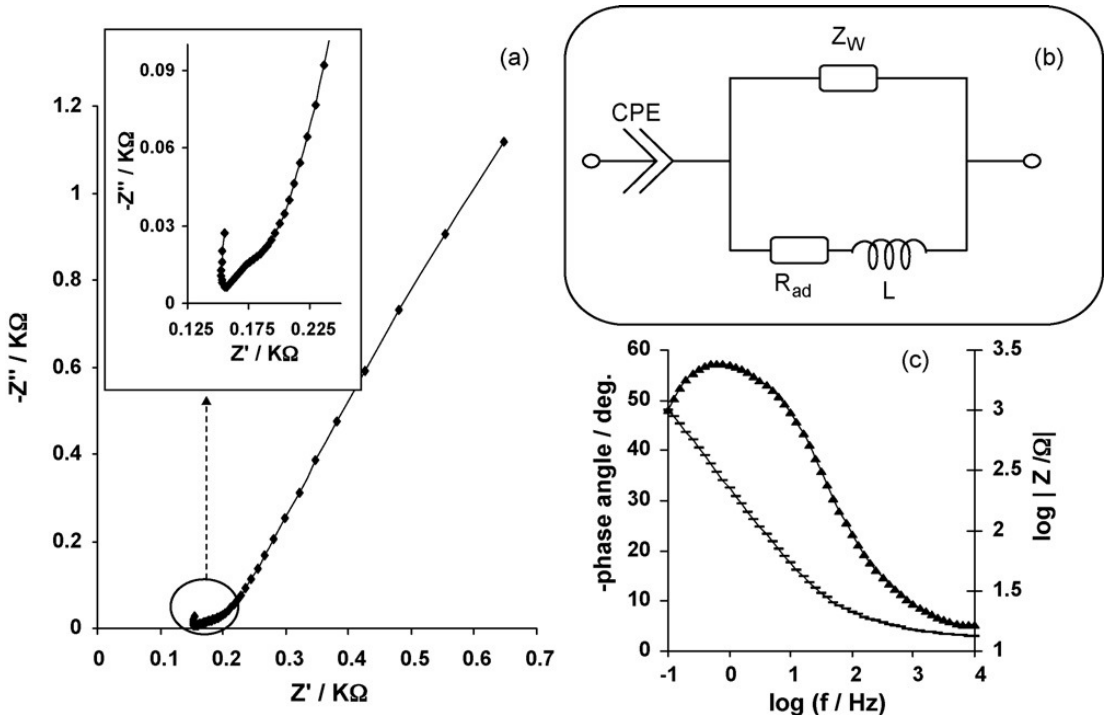

Figure 6.6: (a) Typical Nyquist plots of some electrodes in 1 mM nitrite solution (PBS pH 7.4) at fixed potential of 0.80 V vs Ag|AgCl sat'd KCl. Inset is the enlarged portion of the high frequency region (b) Represents the circuit used in the fitting of the EIS data in 6a (c) Bode plot obtained for EPPGE-SWCNT-Co showing the plot of -phase angle (deg.) vs log (f/Hz).

Table 6.2: Impedance data obtained for the modified EPPGE-SWCNT-Co electrodes in 10^{-3} M NO_2^- (in PBS pH 7.4 and 3.0) at 0.80 V vs Ag|AgCl sat'd KCl.

Electrodes	**Impedimetric Parameters**					
	CPE/ $mFcm^{-2}$	**n**	**10^6Z_w/ Ωcm^2**	**10^6L/ Hcm^2**	**R_{ad} /Ωcm^2**	**pseudo χ^2**
EPPGE-SWCNT-Co (at pH 7.4 PBS)	1.20±0.10	0.73±0.01	1.48±0.02	80. 6±1.43	38.37±0.08	1.02 x 10^{-4}
EPPGE-SWCNT-Co (at pH 3.0 PBS)	9.10±1.40	0.87±0.06	3.21±0.11	2877.93±207.50	73.36±1.26	3.49 x10^{-5}

6.6 Effect of varying scan rate

Cyclic votammetric experiments were carried out with the EPPGE-SWCNT-Co to establish the impact of scan rate (ν) at constant concentration (1 mM) of nitrite at pH 7.4 and 3.0 solutions. In cases, a shift in potential with increase in scan rate (not shown) was observed. From the Randles-Sevčik equation for an anodic oxidation process [18] (Equation 6.4):

$$I_p = 3.01\times10^5 n[(1-\alpha)n_\alpha]^{1/2} A C_b D^{1/2} \nu^{1/2} \quad (6.4)$$

where all symbols have their usual meaning. C_b is nitrite bulk concentration (1 mM). The plot of the peak current (I_p) against the square root of scan rate ($\nu^{1/2}$) (Figure 6.7) for scan rate ranging from 25 to 200 mVs^{-1}, gave a linear relationship (R^2 = 0.9969 for nitrite oxidation at pH 7.4 with approximately zero intercept, confirming a diffusion-controlled process. However, at higher scan rate (> 200 mVs^{-1}), plot of the peak current (I_p) against the square root of scan rate ($\nu^{1/2}$) gave a straight line (R^2 = 0.996) with a negative intercept suggesting that at higher scan rates the reaction is not totally diffusion-controlled. This result supports the earlier discussed adsorption of intermediate products under the EIS study.

Using Tafel equation (Equation 6.5) for a totally irreversible-diffusion controlled process [18], the linear relationship between the peaks potential E_p and the logv (not shown) confirms the chemical irreversibility of nitrite electrocatalytic oxidation process.

$$Ep = \frac{b}{2}\log\nu + const. \quad (6.5)$$

From Equation 6.5, b = Tafel slope = 2.303RT/(1-α)nF where all symbols have their usual meaning. Assuming n = 2 for nitrite, the value of electron transfer coefficient (α) was obtained from Equation 6.5 as 0.72 for nitrite at pH 7.4.

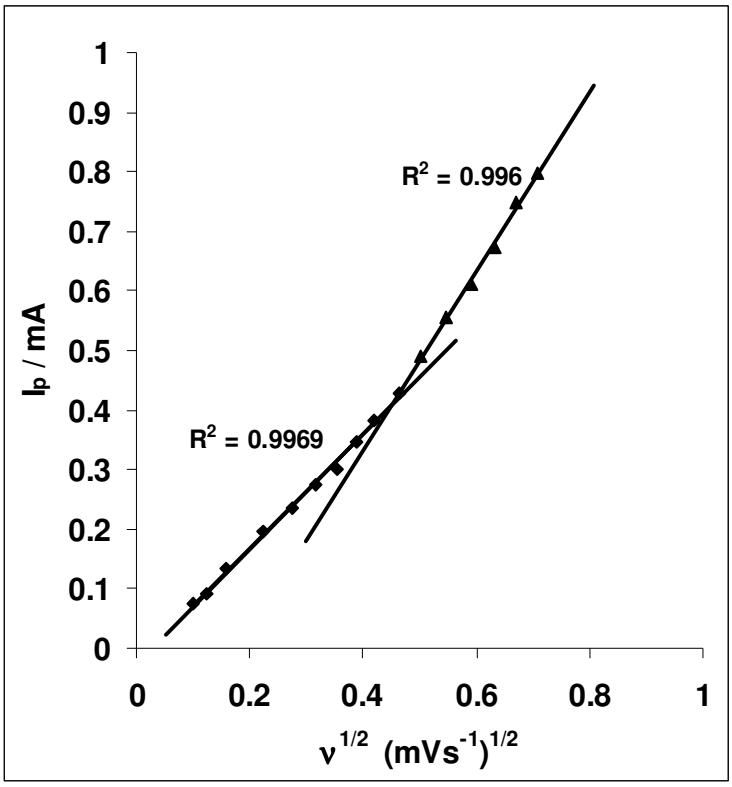

Figure 6.7: Plot of peak current (I_p) versus square root of scan rate ($\nu^{1/2}$) for EPPGE-SWCNT-Co in 0.1M pH 7.4 PBS containing 10^{-3} M nitrite.

Secondly, a Tafel slope of about 240 and 214 $mVDec^{-1}$ at pH 7.4 and 3.0 respectively implies a strong binding of reactants or intermediates on the electrode surface, or reactions occurring within a porous electrode structure [14]. The value agreed with 0.73 reported for cobalt phthalocyanide modified electrode for the oxidation of nitrite [13]. The minimum α value should be 0.5 for all

standard reaction mechanism [19]. α values at approximately 0.5 indicate that there is an equal probability that the reaction activated transition state can form either products or reactants [14]. Thus, α value larger than this indicates a more favoured reaction mechanism [19], which may explain why the electrocatalytic oxidation of nitrite to its oxidation product was more favoured on the EPPGE-SWCNT-Co electrode compared with the bare EPPGE.

6.7 Electroanalysis of nitrite at neutral and acidic pH

Chronoamperometric experiment was carried out by setting the peak potential at which the analyte was best catalysed. The chronoamperogram (Figure 6.8) was obtained by adding different aliquots of the nitrite solution. Using Equation 6.6 [2]:

$$\frac{I_{cat}}{I_L} = \pi^{1/2}\left(kC_o t\right)^{1/2} \qquad (6.6)$$

where all symbols have their usual meaning. From the plot of I_{cat}/I_l vs $t^{1/2}$ (not shown) the catalytic rate constant *K* for EPPGE-SWCNT-Co in pH 7.4 and 3.0 PBS containing 10^{-3}M NO_2^- are (0.32±0.03) and (0.34±0.05) x 10^5 cm^3 $mol^{-1}s^{-1}$ respectively. The results are approximately same as the 2.75 x 10^3 M^{-1} s^{-1} (or 2.75 x 10^6 cm^3 mol^{-1} s^{-1}) reported by Reza *et. al.*, 2006 [20] for the electrocatalytic reduction of nitrite on carbon paste electrode modified with ferricyanide but lower than 7 x 10^5 M^{-1} s^{-1} (or 7 x 10^8 cm^3 mol^{-1} s^{-1}) reported by Natalia et. al., 2005 [21] for catalytic oxidation of nitric oxide and nitrite by water-soluble manganese (III) meso-tetrakis(*N*-methylpyridinium-4-yl) porphyrin (Mn(III)(4-TMPyP) on indium-tin oxide (ITO) electrode in pH 7.4 phosphate buffer solutions. The

difference in the magnitude of *K* could be due to the different electrode modifier and their interaction with the nitrite molecules.

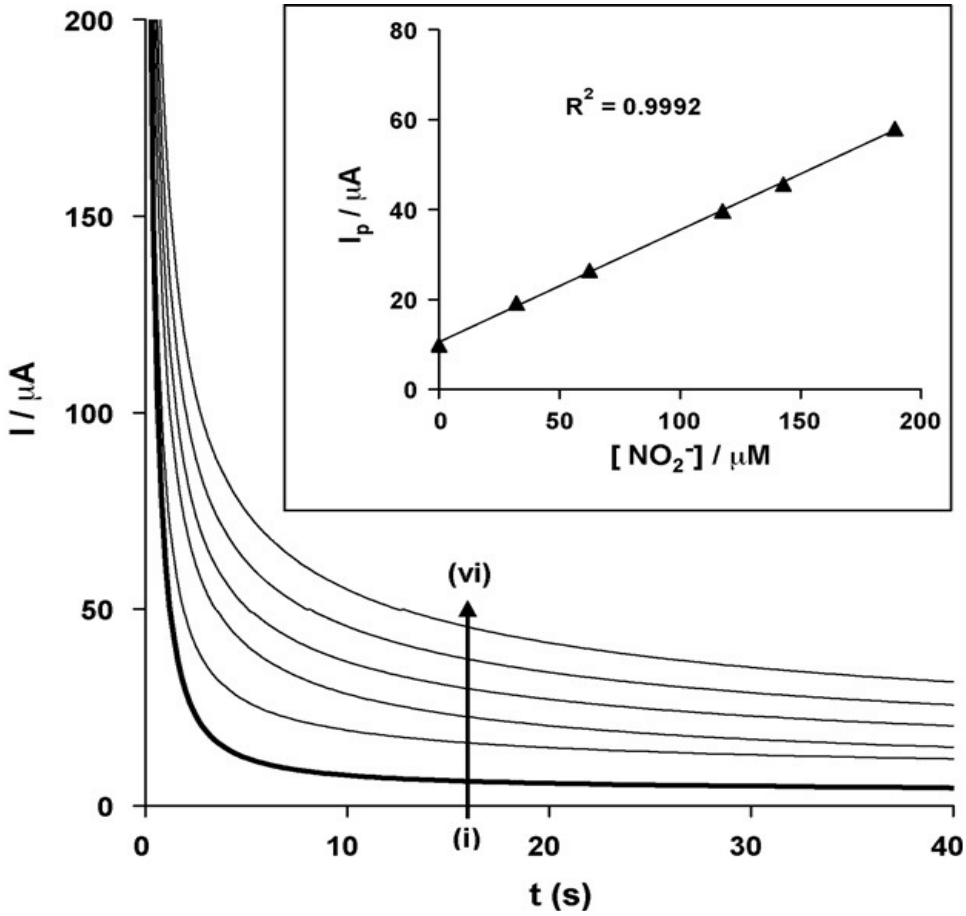

Figure 6.8: Typical examples of chronoamperogram obtained for EPPGE-SWCNT-Co in phosphate buffer solution (pH 7.4) containing different concentrations of nitrite (0.0, 32.3, 62.5, 118.0, 143.0, and 189.0 μM (i to vi)). Inset is typical plot of current response vs nitrite concentration.

Similarly, the plot of I_p versus [NO_2^-] gave the sensitivity values which are (0.250 ± 0.001) μA/μM NO_2^- at pH 7.4 and (0.032 ± 0.001) μA/μM for NO at pH 3.0. The limits of detection (LoD = 3.3 δ/m) are 5.61±0.48 and 8.03±0.68 μM for nitrite and nitric oxide

respectively. The result is in the same μM detection range reported for nitrite and nitric oxide on electropolymerizable iron (III) and cobalt (II) complexes on glassy carbon electrode [22] or indium (III) hexacyanoferate (III) (InHCF) on glassy carbon electrode [23]. Presently, no literature on the electrooxidation of nitrite using this type of electrode has been reported. The sensitivity obtained in this study could be due to the ability of SWCNTs to function as efficient conducting species for the catalytic cobalt nanoparticles. From Langmuir adsorption isotherm theory (Equation 6.7) [24], the plot of the ratio of concentration [nitrite] and the catalytic current I_{cat} ([nitrite] / I_{cat}) against concentration [nitrite] (not shown) gave a straight line which can be interpreted as an adsorption controlled electrochemical process.

$$\frac{[\text{Nitrite}]}{I_{cat}} = \frac{1}{\beta I_{max}} + \frac{[\text{Nitrite}]}{I_{max}} \qquad (6.7)$$

The adsorption equilibrium constant for the EPPGE-SWCNT-Co was estimated as β (9.94 ± 0.05) x 10^3 M^{-1} and (4.80 ± 0.02) x 10^3 M^{-1} for NO_2^- and NO. Thus, the Gibbs free energy change due to adsorption was estimated as -22.81 and -21.00 $kJmol^{-1}$ using Equation 6.8.

$$\Delta G^o = -RT\ln\beta. \qquad (6.8)$$

From the scan rate study and other studies, adsorption of the analyte on the electrode was evident. Further probe into the adsorptive properties of nitrite was carried out using the adsorption

stripping voltammetry. The linear sweep voltammetric evolutions (not shown) of EPPGE-SWCNT-Co in PBS containing different aliquots of nitrite was obtained. Plot of I_p vs $[NO_2^-]$ gave LoD values of 8.4±0.71 and 11.6±0.99 µM for nitrite at pH 7.4 and 3.0. Using Equations 6.7 and 6.8 above, the adsorption equilibrium constant β was estimated as (13.02 ± 0.03) x 10^3 M^{-1} and (56.7 ± 0.01) x 10^3 M^{-1} for nitrite at pH 7.4 and 3.0. Thus, the Gibbs energy change due to the adsorption was estimated as -6.36 and -10.00 $kJmol^{-1}$ for pH 7.4 and 3.0, respectively.

From the result, adsorption of NO_2^- and NO on the electrode followed about the same kinetics based on the insignificant difference in their standard free energy of adsorption (ΔG^o). This is not unexpected since the tendency for the two analytes to interchange is very high, and they both give nitrate (NO_3^-) as their final oxidation product. The adsorption stripping voltammetry technique seems to be more viable for nitrite analysis on the electrode system since the high negative ΔG^o further confirms the strong adsorption of nitrite. From the above discussion, and based on the previous reports on the mechanism of NO_3^- electro-oxidation at modified electrodes [25], it is assumed that the electrocatalytic response of NO_3^- at EPPGE-SWCNT-Co in aqueous solutions follows a similar mechanism:

$$[\text{SWCNT-Co}]_{film} + H_2O \longrightarrow [\text{SWCNT-Co}^{2+}]_{film\ (aq)} + e^- \quad (6.9)$$

$$[\text{SWCNT-Co}^{2+}]_{film} + NO_2^- \rightleftharpoons [\text{SWCNT-Co}^{2+}\text{---}(NO_2^-)]_{adduct} \quad (6.10)$$

$$[\text{SWCNT-Co}^{2+}\text{---}(NO_2^-)]_{adduct} \rightleftharpoons [\text{SWCNT-Co}^{3+}]_{film} + NO_2 + e^- \ (\text{slow}) \quad (6.11)$$

$$2NO_2 + H_2O \rightleftharpoons 2H^+ + NO_3^- + NO_2^- \quad (6.12)$$

$$NO_2^- + H_2O \longrightarrow 2H^+ + NO_3^- + 2e^- \quad (6.13)$$

$$[\text{SWCNT-Co}^{3+}]_{film} + e^- \longrightarrow [\text{SWCNT-Co}^{2+}]_{film} \quad (6.14)$$

The nitrite ion interact with the SWCNT-confined Co(II) film forming an adduct (Equation 6.10). This step represents the adsorption process. Equation 6.11 is assumed to be the rate-determining step which is a one-electron process. The oxidation of the Co(II) to Co(III) simultaneously leads to the generation of the nitrogen dioxide. The formation of the NO_2 (Equation 6.11) is followed by its disproportionation to give nitrite and nitrate (Equations 6.12 and 6.13). Co(III) is reduced to regenerate the Co(II) (Equation 14).

In a related study, the surface electrochemistry of synthesised Co and Co_3O_4 nanoparticles as well as their electrocatalytic detection ability towards nitrite on EPPGE platform was explored. Surprisingly most work focus more on electrocatalysis of the metal nanoparticles other than their electron transport behaviour that form the basis for electrocatalysis. The prime motivating factor for carrying out this study is the ability to produce nano-scaled cobalt and cobalt oxides in high commercial quantity compared to the commercially unvailable quantity from the electrodeposition method. Figures 6.9a and b showed the comparative transmission electron microscopy (TEM) images of Co (a) and the Co_3O_4 nanoparticles while (b) while Figure 6.9c and d are their corresponding FESEM images. The Co nanoparticles form amorphous nanoparticles or nanowires (Figures 6.9a and 6.9c). On the other hand, Co_3O_4 nanoparticles appeared crystalline (Figure 6.9b). The crystals aggregated and form a web-like structure (Figure 6.9d). From the TEM result, the size of most of the particles is in 20 to 50 nm for Co and 10 to 30 nm for the Co_3O_4.

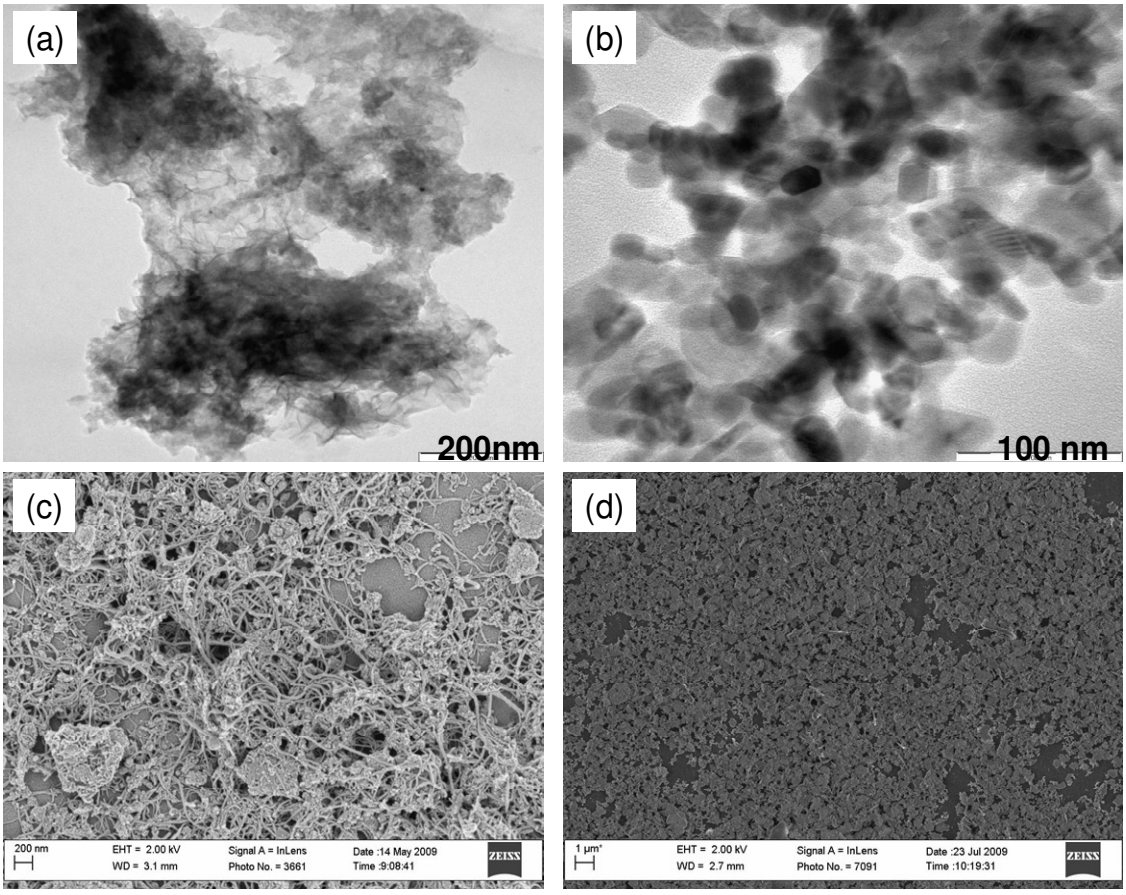

Figure 6.9: TEM images of (a) Co and (b) Co_3O_4 nanoparticles. Figures 6.9c and d are the FESEM micrographs of Co and Co_3O_4 nanoparticles, respectively.

The XRD spectra for the nanosized particles are shown in Figure 6.10. The nanoscaled Co (Figure 6.10a) is characterised by XRD peaks at 2θ of 47.9°, 59.8° and 79.6° which could be assigned to (111), (200) and (222) of a cubic structures Co nanoparticles [26,27]. The Co_3O_4 nanaoparticles (Figure 6.10b) show characteristic peaks at 2θ of 22.1, 36.5, 43.1, 45.1, 52.5, 57.7, 65.7, 70.2 and 77.5 due to the indices of (111), (220), (311), (222), (400), (331), (422), (511) and (440) corresponding to Cubic Fd-3m Co_3O_4 crystal

lattice [27,28]. From Debye-Scherrer equation [29,30], average crystalite size of 22.8 nm was obtained which is in consistent with the TEM result.

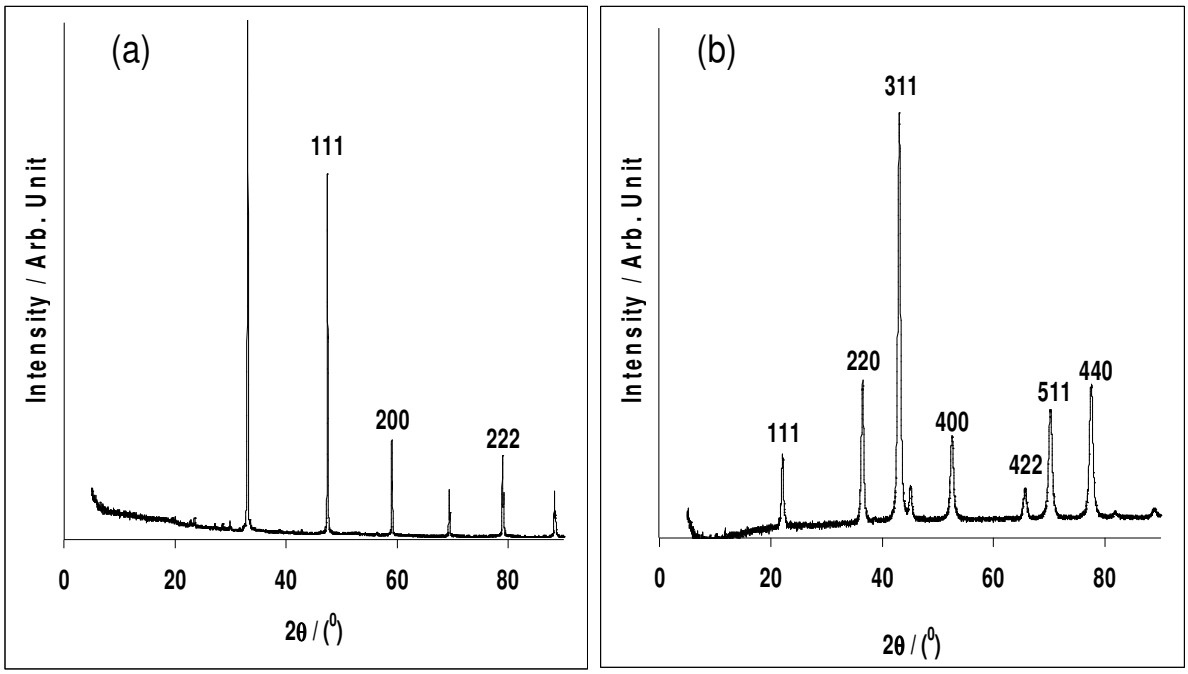

Figure 6.10: XRD spectra of Co (a) and Co_3O_4 (b) nanoparticles.

Figure 6.11 compares the current response of the bare and the modified electrodes in (a) 0.1 M PBS (pH 7.0) and (b) 5 mM $Fe(CN)_6]^{4-}$/$[Fe(CN)_6]^{3-}$ solution. In Figure 6.11a, the electrode based on the Co nanoparticles showed broad anodic peak at *ca* 0.6 V, presumable due to the formation of Co_3O_4 through the reaction represented in Equation 6.1 above.

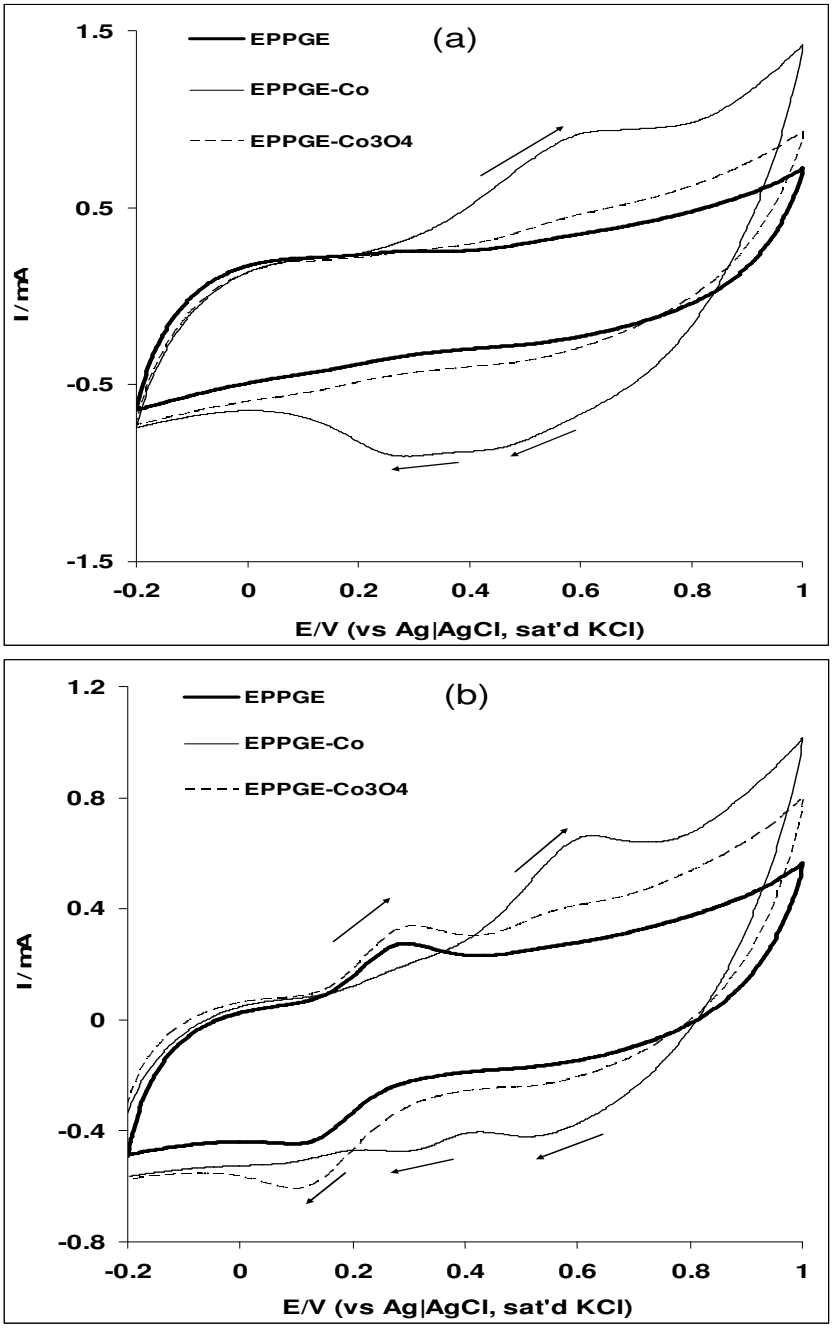

Figure 6.11: Comparative cyclic voltammetric evolutions of the EPPGE, EPPGE-Co and EPPGE-Co_3O_4 electrodes in (a) 0.1 M PBS (scan rate = 100 mVs^{-1}), and (b) 5 mM $[Fe(CN)_6]^{4-}/[Fe(CN)_6]^{3-}$ solution in pH 7.0 PBS (scan rate = 50 mVs^{-1}).

The broadness of the peak may be due to the formation of other oxidation products (Equation 6.2). The cathodic peaks observed at ca 0.52 and 0.22 V are attributed to the reduction of CoOOH to $Co(OH)_2$ or Co_3O_4. Interestingly, the electrodes based on the Co_3O_4 nanoparticles did not show recognisable redox process as the Co nanoparticles in the neutral pH conditions used.

Next, the extent to which these electrodes mediate the electron transport of the redox probe, $Fe(CN)_6]^{4-}/[Fe(CN)_6]^{3-}$, to and from the underlying electrodes was questioned. Two redox couples are noticed for the electrodes in $Fe(CN)_6]^{4-}/[Fe(CN)_6]^{3-}$ solution (Figure 6.11b); the redox couples in the 0 – 0.3 V region being attributed to the $Fe(CN)_6]^{4-}/[Fe(CN)_6]^{3-}$ redox process, while the redox couples in the 0.3 – 0.7 V region correspond to cobalt processes. Electrochemical impedance spectroscopy (EIS) experiment was carried at fixed potential of 0.2 V (the equilibrium potential, $E_{1/2}$, of the $[Fe(CN)_6]^{4-}/[Fe(CN)_6]^{3-}$ couple). The Nyquist plot obtained (Figure 6.12) was satisfactorily fitted using the modified Randles electrical equivalent circuit model shown in the inset. The R_{ct} values follow the trend: EPPGE-Co (0.36 Ωcm^2) < EPPGE-Co_3O_4 (0.60 Ωcm^2) << bare-EPPGE (1.23 Ωcm^2) (Table 6.3). The modified electrodes showed lower R_{ct} values compared to the bare EPPGE, indicating that the nanoparticle catalysts enhance electron transfer of the redox probe compared to the unmodified EPPGE.

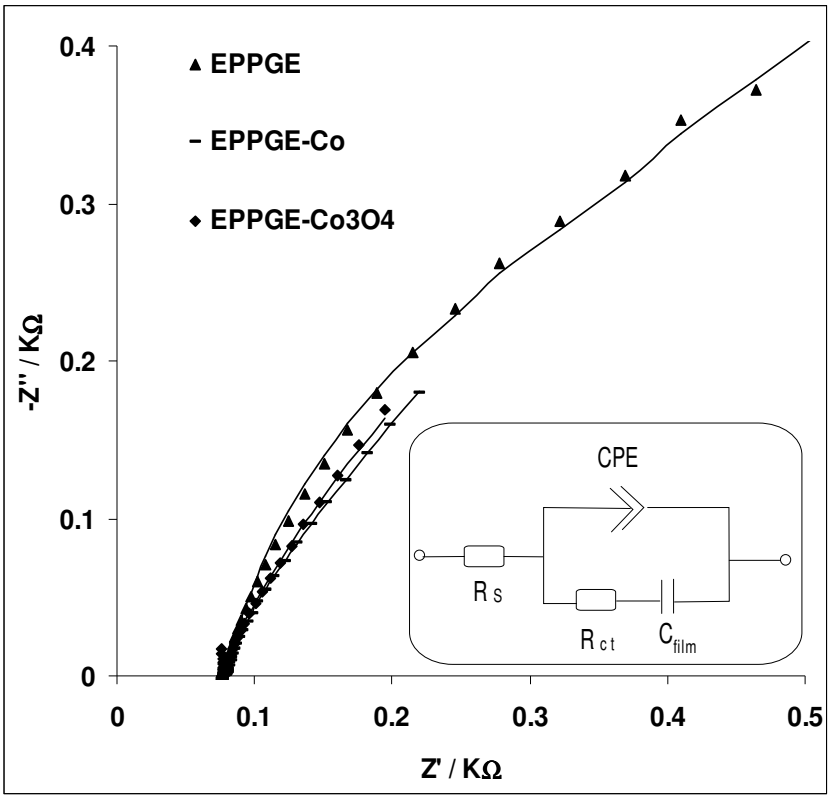

Figure 6.12: Typical Nyquist plots obtained for the electrodes in 5 mM $[Fe(CN)_6]^{4-}$ / $[Fe(CN)_6]^{3-}$ solution at a fixed potential of 0.2 V (vs Ag|AgCl, sat'd KCl). Inset in Figure 6.12 is the circuit used in the fitting of the EIS data.

Table 6.3: Impedance data obtained for EPPGE, EPPGE-Co and EPPGE-Co_3O_4 electrodes in 5 mM $Fe(CN)_6]^{4-}$/$[Fe(CN)_6]^{3-}$ solution at 0.2 V (vs Ag|AgCl sat'd KCl).

Electrodes	**Impedimetric Parameters**				
	R_s/ Ωcm^2	**CPE/ μFcm^{-2}**	**N**	**R_{ct}/ Ωcm^2**	**C_{film}/ mFcm^{-2}**
EPPGE	7.02±0.01	0.82±0.35	0.40±0.01	1.23±0.02	3.09±0.11
EPPGE-Co	7.80±0.01	216.40±25.47	0.50±0.01	0.36±0.01	13.02±0.34
EPPGE-Co_3O_4	7.57±0.01	381.3±13.01	0.52±0.05	0.60±0.04	15.98±3.77

At 2.5 mg/mL Co loading, the current responses in NO_2^- follow the order: bare EPPGE (43.7 μA) > EPPGE-CoO (21.0 μA) > EPPGE-Co (18.0 μA) (Figure 6.13). The result agreed with the recent report by Compton group [31] in terms of onset potential of catalysis and the peak potential for nitrite oxidation on bare glassy carbon electrode. However, at 7.5 mg/mL Co and Co_3O_4 loading, EPPGE-Co gave the highest current response (83.0 μA) with lower onset potential (0.3 V) of catalysis which is ~ 380 mV lower than *ca* 0.67 V recorded for the other electrodes (Figure 6.13). At this loading, its current response was ~ 2 times the bare EPPGE and 2.5 times EPPGE-CoO. Thus, contribution of modified electrode to reducing nitrite overpotential on bare electrode, and in enhancing its oxidation current are a possibility, which may depend on the method of modification, the nature of the electrocatalyst and amount used in modifying the electrode.

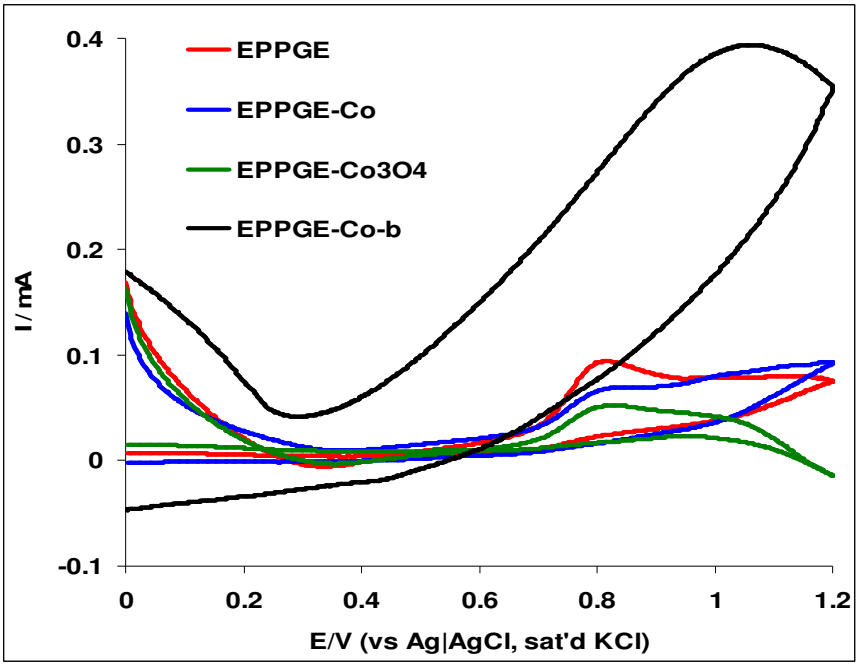

Figure 6.13: Comparative current response of (a) EPPGE, EPPGE-Co and EPPGE-Co_3O_4 (after background current subtraction) in pH 7.4 PBS containing 1.0 mM NO_2^- solution (scan rate = 25 mVs^{-1}). EPPGE-Co-b represents 7.5 mg/mL Co loading in pH 7.4 PBS containing 1.0 mM NO_2^- solution.

The results here also show enhanced electrochemical performance compared to several reports, including the earlier work above incorporating carbon nanotubes in terms of onset potentials and current response. Surprisingly, attempts to use CNTs as supports for these synthesised Co and Co_3O_4 nanoparticles did not improve the electrochemistry of nitrite, a further advantage of these metal nanoparticles over their electrodeposited counterparts that require CNTs. Since EPPGE-Co electrode proved to be better towards nitrite oxidation, all further studies were carried out with it, unless otherwise stated.

The catalytic behaviour of the electrodes towards nitrite oxidation was also investigated using EIS. The Nyquist plots obtained for the electrodes during nitrite oxidation at pH 7.4 (at fixed potential of 0.8 V vs Ag|AgCl, sat'd KCl) is presented in Figure 6.14. A modified Randles circuit model already discussed above (inset in Figure 6.12) satisfactorily fitted the data from nitrite oxidation (Table 6.4). The C_{film} is replaced by C_{ads} which is attributed to the high capacitive nature of the synthesised Co and Co_3O_4 nanoparticles or adsorption of NO_2^- intermediate product on the electrode. The low R_{ct} of the EPPGE-Co (0.31 Ωcm^2) compared with the bare EPPGE (0.36 Ωcm^2) and EPPGE-Co_3O_4 (0.46 Ωcm^2) also explain the good electron transport and catalysis witness at the electrode.

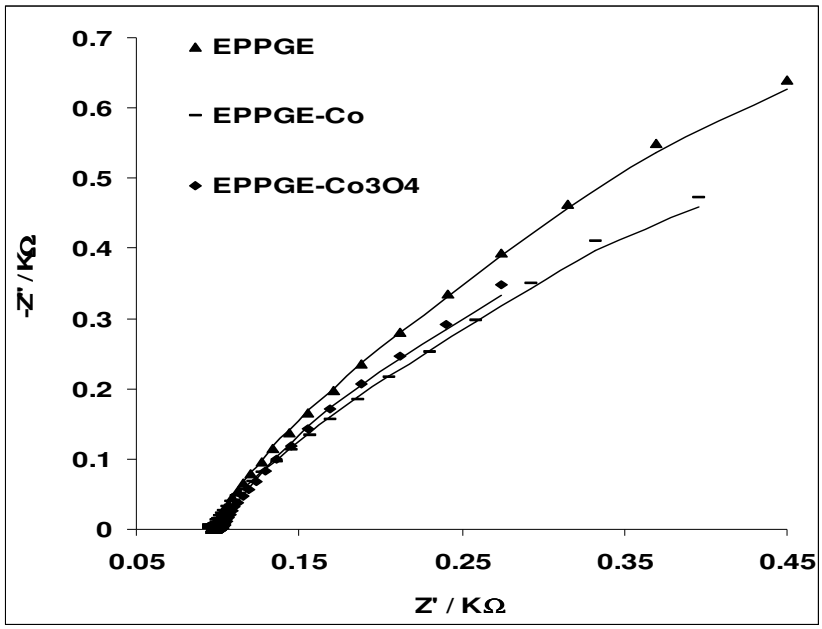

Figure 6.14: Typical Nyquist plots obtained for EPPGE, EPPGE-Co and EPPGE-Co_3O_4 in 1.0 mM NO_2^- solution at a fixed potential of 0.8 V (vs Ag|AgCl, sat'd KCl).

Table 6.4: Impedance data obtained for some of the electrodes in 1.0 mM NO_2^- (in PBS pH 7.4 at 0.80 V vs Ag|AgCl sat'd KCl.

Electrodes	**Impedimetric Parameters**				
	$R_s/\Omega cm^2$	**$CPE/\mu Fcm^{-2}$**	**N**	**$R_{ct}/\Omega cm^2$**	**$C_{ads}/mFcm^{-2}$**
EPPGE	9.48±0.01	133.8±35.39	0.59±0.01	0.36±0.01	6.98±0.30
EPPGE-Co	9.31±0.01	170.6±48.80	0.57±0.01	0.31±0.01	6.83±0.43
EPPGE-Co_3O_4	10.00±0.01	160.4±42.17	0.55±0.02	0.46±0.01	17.07±0.87

Cyclic voltammograms showing the current responses in NO_2^- with increasing scan rates were also studied (25 – 500 mVs^{-1}). A shift in potential with increase in scan rate was observed. The plot of the peak current (I_p) against the square root of scan rate ($\nu^{1/2}$) gave a linear relationship (R^2 = 0.9915) with a positive intercept, suggesting a diffusion-controlled process. There was a linear relationship between the peak potential E_p and the logν (not shown), which confirms the chemical irreversibility of nitrite electrocatalytic oxidation process. The value of the Tafel slope is somewhat huge (540.8 mV dec^{-1}) compared to the normal reported values for various analytes including nitrite on SWCNT-Co modified electrode. As earlier mentioned, high Tafel values generally indicate binding of the analyte or its intermediates on the electrode surface, or reactions occurring within a porous electrode structure [14,32]. From the above discussion, the electrocatalytic response of NO_2^- at EPPGE-Co followed the same mechanism as proposed in Equations 6.9 to 6.14 above.

Next, the effect of current response on varying concentrations of nitrite using chronamperometric technique (Figure 6.15) was studied. Plot of current response versus nitrite concentration (inset in Figure 6.15) gave a linear relationship (Y = (1.32±0.01)X + 16.82±0.29 (R^2 = 0.9996)) and sensitivity of 1.32±0.01 μA μM^{-1}. The limit of detection (LoD = 3.3 δ/m) was calculated as 0.73±0.06 μM. The 0.73 μM detection limit obtained is about 8 times lower than reported for the SWCNT-Co modified electrode reported. Nitrite at neutral pH has been detected at 4.0 μM using thionin/multiwalled carbon nanotubes/glassy carbon modified electrode [33] and myoglobin/ZnO/graphite modified electrode [34], 1.2 μM on haemoglobin/colloidal gold

nanoparticles/TiO_2-sol gel film/GCE modified electrode [35]. From the plot of I_{cat}/I_l vs $t^{1/2}$ (not shown) the catalytic rate constant for nitrite was obtained as (2.32±0.20) x 10^6 cm^3 $mol^{-1}s^{-1}$. This result is close to the 6.03 x 10^6 $M^{-1}s^{-1}$ reported for the electrocatalytic reduction of nitrite at Vanadium–Schiff base complex/MWCNTs modified GC electrode [36].

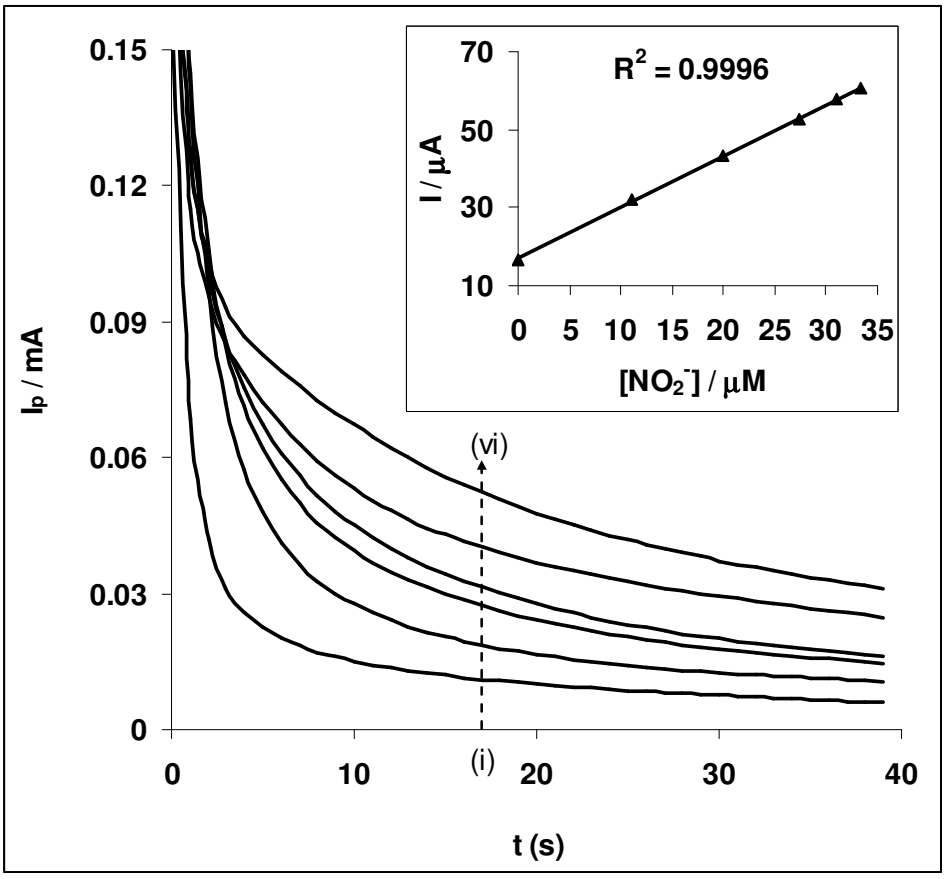

Figure 6.15: Typical chronoamperogram of EPPGE-Co in (a) 0.1 M PBS pH 7.4 containing different concentration of NO_2^- (0.0, 11.1, 20.0, 27.3, 31.0 and 33.3 µM (i to vi)). Inset is the plot of peak current (I_p) versus NO_2^- concentrations.

This study showed that the Co nanoparticle modified electrodes exhibited faster electron transfer behaviour in $[Fe(CN)_6]^{3-/4-}$ redox probe than their corresponding nano-oxides. The high charge transfer resistance of the cobalt oxide modified electrodes have been attributed to surface passivation and low surface active materials. EPPGE-SWCNT-Co has the fastest electron transport, aided by the electrical conducting single-walled carbon nanotubes which form a synergistic effect with the cobalt nanoparticles. In the contrary, attempts to use CNTs as supports for synthesised Co and Co_3O_4 nanoparticles did not improve the electrochemistry of nitrite, a further advantage of these metal nanoparticles over their electrodeposited counterparts that require CNTs. The detection and the electro-catalytic oxidation of nitrite were successful on all the electrodes studied. In both electrodeposition and synthesis experiment, EPPGE-SWCNT-Co or EPPGE-Co gave the highest current response, and at lower potential compared with other electrodes investigated. The electrocatalytic-oxidation of nitrite on the electrode followed adsorption-controlled electrochemical process with complex impedance behaviour. There is no significant difference in the standard free energy change (ΔG^0) due to adsorption, suggesting that the adsorption of NO_2^- and NO on the EPPGE-SWCNT-Co followed about the same mechanism. The study showed that, using this kind of electrode system for sensing and analytical application requires a special caution since the adsorptive nature of the electrode may have an effect on its sensing properties towards the analyte.

References

1. A. Salimi , H. Mamkhezri, R. Hallaj , S. Soltanian, *Sens. Actuators B* 129 (2008) 246.

2. A. Salimi, R. Hallaj, S. Soltanian, H. Mamkhezri, *Anal. Chim. Acta* 594 (2007) 24.

3. J. Zagal, M. Paez, A.A. Tanaka and J.R. dos Santos Jr, C.A. Linkous, *J. Electroanal Chem.* 339 (1992) 13.

4. S. Zecevic, B. Simic-Glavaski, E. Yeager, A.B.P. Lever and P.C. Minor, *J. Electroanal. Chem.* 196 (1985) 339.

5. A.B.P. Lever, S. Liccocia, K. Magnell, P.C. Minor and B.S. Ramaswamy, *Am. Chem. Sot. Symp.Ser.* 201 (1982) 237.

6. S. Sunohara, K. Nishimura, K. Yahikozawa, M. Ueno, *J. Electroanal. Chem.* 354 (1993) 161.

7. H. Kasurk, G. Nurk, E. Lust, *J. Electroanal. Chem.* 613 (2008) 80.

8. W. Lajnef, J.-M. Vinassa, S. Azzopardi, O. Briat, E. Woirgard, C. Zardini, J.L. Aucouturier, *PESC* 04 1 (2004) 131.

9. M.E. Orazem, B. Tribollet, *Electrochemical Impedance Spectroscopy*, John Wiley & Sons Inc, Hoboken, NJ., 2008, Chapter 13.

10. C. Yang, Q. Lu, S. Hu, *Electroanalysis* 18 (2006) 2188.

11. M. Thamae, T. Nyokong, *J. Electroanal. Chem.* 470 (1999) 126.

12. P. Tau, T. Nyokong, *Electrochim. Acta* 52 (2007) 4547.

13. F. Matemadombo, T. Nyokong, *Electrochim. Acta* 52 (2007) 6856.

14. B.O. Agboola, T Nyokong, *Anal. Chim. Acta* 587 (2007)116.

15. J. Bisquert, H. Randriamahazaka, G.Garcia-Belmonte, *Electrochim. Acta* 51 (2005) 627.

16. M. Jafarian, M. G. Mahjani, H. Heli, F. Gobal, H. Khajehsharifi, M. H. Hamedi, Electro*chim. Acta* 48 (2003) 3423.

17. S. Majdi, A. Jabbari, H. Heli, A. A. Moosavi-Movahedi, *Electrochim. Acta* 52 (2007) 4622.

18. A.J. Bard, L.R. Faulkner, Electrochemical Methods: *Fundamentals and Applications*, 2nd ed., John Wiley & Sons, Hoboken, NJ., 2001.

19. J.N. Soderberg, A.C. Co, A.H. C. Sirk, V.I. Birss, *J. Phys. Chem. B* 110 (2006) 10401.

20. R. Ojani, J-B, Raoof, E. Zarei, *Electrochim. Acta* 52 (2006) 753.

21. N.S. Trofimova, A.Y. Safronov, O. Ikeda, *Electrochim. Acta* 50 (2005) 4637.

22. K.I. Ozoemena, Z. Zhao, T. Nyokong, *Inorg. Chem. Commun.* 9 (2006) 223.

23. E. Casero, J. Losada, F. Pariente, E. Lorenzo, *Talanta* 61 (2003) 61.

24. H.X. Ju, L. Donal, *J. Electroanal. Chem.* 484 (2000) 150.

25. F. Armijo, M.C. Goya, M. Reina, M.J. Canales, M.C. Arevalo, M.J. Aguire, *J. Mol. Cat. A*: 268 (2007) 148.

26. H. Shao, Y. Huang, H. Lee, Y.J. Suh, C.O. Kim, *Current Applied Physics* 6S1 (2006) e195.

27. M. Salavati-Niasari, Z. Fereshteh, F. Davar, *Polyhedron* 28 (2009) 1065.

28. M. Salavati-Niasari, F. Davar, M. Mazaheri, M. Shaterian *J. Magnetism Magnetic Materials* 320 (2008) 575.

29. Y-K. Sun, M. Ma, Y. Zhang, N. Gu, Coll. Surf. A: *Physicochem. Eng. Aspects* 245 (2004) 15.

30. R.M. Cornell, U. Schertmann, Iron Oxides in the laboratory: Preparation and Characterization, VCH, Weinheim (1991).

31. B.R. Kozub, N.V. Rees, R.G. Compton, *Sens. Actuat. B* 143 (2010) 539.

32. J.N. Soderberg, A.C. Co, A.H.C. Sirk, V.I. Birss, *J. Phys. Chem. B* 110 (2006) 10401.

33. A. Salimi, A. Noorbakhash, F.S. Karonian, *Int. J. Electrochem. Sci.* 1 (2006) 435.

34. G. Zhao, J.J. Xu, H.Y. Chen, *Anal. Biochem.* 350 (2006) 145.

35. W. Yang, Y. Bai, Y. Li, C. Sun, *Anal. Bioanal. Chem.* 382 (2005) 44.

36. A. Salimi, H. Mamkhezri, S. Mohebbi, *Electrochem. Commun.* 8 (2006) 688.